

# AstroSpy: On detecting Fake Images in Astronomy via Joint Image-Spectral Representations

Mohammed Talha Alam<sup>\*†1</sup>, Raza Imam<sup>†1</sup>, Mohsen Guizani<sup>1</sup>, Fakhri Karray<sup>1</sup>

<sup>1</sup>Mohamed bin Zayed University of Artificial Intelligence, Abu Dhabi, UAE

The prevalence of AI-generated imagery has raised concerns about the authenticity of astronomical images, especially with advanced text-to-image models like Stable Diffusion producing highly realistic synthetic samples. Existing detection methods, primarily based on convolutional neural networks (CNNs) or spectral analysis, have limitations when used independently. We present AstroSpy, a hybrid model that integrates both spectral and image features to distinguish real from synthetic astronomical images. Trained on a unique dataset of real NASA images and AI-generated fakes (approximately 18k samples), AstroSpy utilizes a dual-pathway architecture to fuse spatial and spectral information. This approach enables AstroSpy to achieve superior performance in identifying authentic astronomical images. Extensive evaluations demonstrate AstroSpy's effectiveness and robustness, significantly outperforming baseline models in both *in-domain* and *cross-domain* tasks, highlighting its potential to combat misinformation in astronomy.

## 1 Introduction

The authenticity of visual data is paramount in scientific fields, particularly in astronomy, where images are central to research, discovery, and public engagement. However, the advent of sophisticated AI models capable of generating highly realistic images has led to a surge in fake astronomical visuals. These fake images can deceive the public, mislead researchers, and potentially disrupt scientific communication. The challenge lies in developing robust methods to discern real images from AI-generated fakes, ensuring the integrity of visual data [1–4]. Given the increasing realism of these fake images, the need for robust detection methods is more urgent than ever [5].

**Motivation** Misleading images can undermine public trust in scientific findings and hinder scientific progress [6–8]. This can affect the allocation of resources and funding. For instance, if AI-generated

images depicting spectacular but fictitious celestial phenomena capture the public's imagination, funding bodies might divert resources away from legitimate scientific research to capitalize on the public interest. This shift can undermine genuine scientific inquiry and the development of accurate astronomical knowledge. Additionally, generated images, while potentially valuable for outreach, must be clearly distinguished from actual data to maintain scientific integrity [9]. The artistic interpretation of astronomical data, such as infrared imagery, already involves some level of abstraction and creativity, but it is grounded in real observations and scientific analysis, which differs fundamentally from wholly fabricated images [10].

**Related Works** Detecting fake images has been extensively studied in digital forensics and deepfake detection, with CNNs being pivotal due to their ability to learn complex image features [11–13]. However, these models often struggle with sophisticated forgeries. Spectral analysis, which examines frequency domain features, has shown promise in detecting anomalies [14–16]. Durall et al. [17] emphasized the importance of frequency domain analysis in detecting GAN-generated images, noting that many GANs fail to reproduce the spectral distributions of real images accurately. Similarly, [18] leveraged frequency domain information to detect manipulated images. Our work bridges these approaches by combining spatial and spectral features to address the unique challenges of detecting fake astronomical imagery.

**Contribution** Recognizing the limitations of these approaches when used in isolation, (1) we introduce AstroSpy, a novel model that integrates both spectral and image features to enhance the detection of fake astronomical images. (2) We utilize a robust dataset composed of real astronomical images from NASA and AI-generated fakes sourced from the 'Raw\_Aug\_HR' and 'T2I\_Aug\_HR' datasets within the FLARE [19] framework. This diverse dataset is crucial for effectively training and evaluating our detection

\*Corresponding author: mohammed.alam@mbzuai.ac.ae

†Equal Contribution

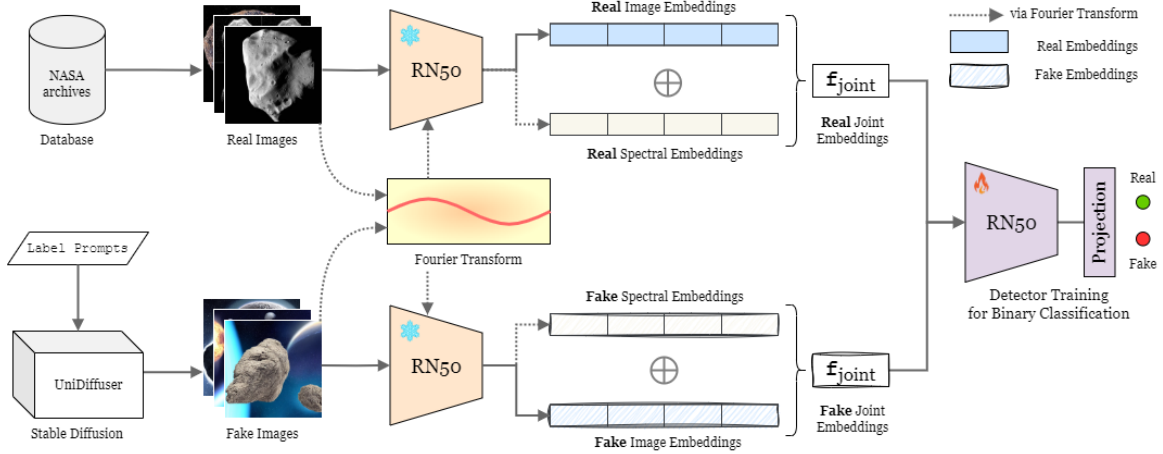


**Figure 1:** AstroSpy architecture: Real images from database archive, and fake images generated by Stable Diffusion, are transformed into spectral embeddings using Fourier Transform. Both image and spectral features are extracted using ResNet50, concatenated into joint embeddings, and used to train a binary classifier for detecting real and fake images.

models. (3) Through extensive experiments, including the creation of *out-of-domain* datasets using UniDiffuser [20], Roentgen [21], and StyleGAN2 [22] for natural images, medical images, and faces, we demonstrate that AstroSpy significantly outperforms existing methods in both *in-domain* and *cross-domain* scenarios.

## 2 Method: AstroSpy

AstroSpy’s workflow leverages a novel combination of image and spectral features to detect fake astronomical images.

### 2.1 Dataset Preparation

We extracted real astronomical images from NASA’s archives using keywords such as planet, star, nebula, galaxy, constellation, black hole, and asteroid, followed by different augmentations, making a comprehensive set of about  $\sim 9k$  real samples. For generating fake samples, we utilized a multi-modal stable diffusion method [23]. By prompting the class labels, we generate  $\sim 9k$  synthetic images that closely mimic the context and visual content of the real samples.

### 2.2 Joint Embeddings

**Image Features:** We utilize a base ResNet50 encoder for extracting image features. ResNet50 is renowned for its deep architecture and ability to capture intricate visual patterns [24]. Let  $I$  represent the input image, and  $F_{\text{ResNet50}}(I)$  denote the feature vector obtained from the ResNet50 encoder:

$$\mathbf{f}_{\text{image}} = F_{\text{ResNet50}}(I) \quad (1)$$

**Spectral Features:** For spectral analysis, grayscale images undergo a Fourier transform [25] to convert them into the frequency domain. Let  $G(I)$  represent the grayscale image derived from  $I$ , and  $\mathcal{F}(G(I))$  denote the Fourier transform of the grayscale image. The magnitude spectrum of the Fourier transform is computed, and these spectral features are processed using the ResNet50 encoder. Let  $F_{\text{ResNet50}}(\mathcal{M})$  denote the feature vector obtained from the magnitude spectrum  $\mathcal{M}$  of the Fourier transform:

$$\mathbf{f}_{\text{spectral}} = F_{\text{ResNet50}}(\mathcal{M}), \quad \text{where } \mathcal{M} = |\mathcal{F}(G(I))| \quad (2)$$

The final joint embedding  $\mathbf{f}_{\text{joint}}$  is obtained by concatenating the image and spectral feature vectors:

$$\mathbf{f}_{\text{joint}} = [\mathbf{f}_{\text{image}} \odot \mathbf{f}_{\text{spectral}}] \quad (3)$$

where  $\odot$  indicates a concatenation function. For AstroSpy, we concatenated  $\mathbf{f}_{\text{image}}$  and  $\mathbf{f}_{\text{spectral}}$  using addition operation. This joint embedding  $\mathbf{f}_{\text{joint}}$  is then fed into a trainable model (like ResNet50 or DenseNet121) followed by fully connected layer for binary classification:

$$\hat{y} = \sigma(\mathbf{W}\mathbf{f}_{\text{joint}} + \mathbf{b}) \quad (4)$$

where  $\sigma$  represents the sigmoid activation function,  $\mathbf{W}$  is the weight matrix,  $\mathbf{b}$  is the bias vector, and  $\hat{y}$  is the predicted probability of the input image being real.

### 2.3 Training Procedure

AstroSpy utilizes the binary cross-entropy loss used to measure the discrepancy between the predicted probabilities  $\hat{y}$  and the actual labels  $y$  as:

$$\mathcal{L} = -[y \log(\hat{y}) + (1 - y) \log(1 - \hat{y})] \quad (5)$$

The gradients of the loss function with respect to the model parameters are computed and used to update the parameters iteratively using the Adam optimizer:

$$\theta \leftarrow \theta - \eta \nabla_{\theta} \mathcal{L} \quad (6)$$

where  $\theta$  represents the model parameters,  $\eta$  is the learning rate, and  $\nabla_{\theta} \mathcal{L}$  is the gradient of the loss function with respect to the parameters. Through this training, AstroSpy learns to accurately distinguish between real and fake astronomical images.

## 3 Results and Discussion

### 3.1 Experiments

**Datasets** We use a curated dataset from [19], containing approximately 9k real samples and 9k synthetic samples across eight classes: Planet, Asteroid, Nebula, Comet, Star, Black Hole, Galaxy, and Constellation. The real samples are sourced from NASA’s archives, while synthetic samples are generated using Stable Diffusion [26]. The dataset is split into training, validation, and test sets in an 80-10-10 ratio. For *out-of-domain* evaluation, we included real samples from ImageNet (natural images) [27], MIMIC (medical images) [28], and FairFace (face images) [29], with corresponding synthetic samples generated by UniDiffuser, Roentgen, and StyleGAN2, respectively.

**Implementation Details** AstroSpy is implemented using PyTorch [30] with two parallel ResNet50 models, one for image features and one for spectral features. Images are resized to 224×224 pixels for both pathways. The final fully connected layer of each ResNet50 is replaced with an identity layer to use the output as feature vectors. The model is trained with a batch size of 32, using the Adam optimizer at a learning rate of 2e-5, and cross-entropy loss for binary classification. Data augmentation techniques such as random rotations, flips, color jittering, and Gaussian blurring are applied to enhance robustness. Early stopping with a patience of 5 epochs is employed to prevent overfitting. Training is conducted for 25 epochs on a single NVIDIA A100 40GB GPU.

### 3.2 In-Domain Generalization

AstroSpy’s *in-domain* generalization capabilities were thoroughly evaluated using a test set comprising real and synthetic astronomical images. The evaluation aimed to determine how well AstroSpy distinguishes between authentic and generated images within the same domain as the training data. The results, as shown in Table 1, demonstrate that AstroSpy significantly outperforms baseline models that use only im-

age or spectral features. AstroSpy achieves an accuracy of 98.5%, highlighting the effectiveness of concatenating both feature types.

### 3.3 Generalization to Out-of-Domain Distributions

AstroSpy’s ability to generalize to entirely different domains was tested using samples generated by UniDiffuser, Roentgen, and StyleGAN2. These samples include natural images, medical images, and face images from various ethnicities, respectively as shown in Figure 4. AstroSpy consistently outperformed baseline models as shown in Table 1, demonstrating its adaptability to different types of images beyond the astronomical domain. This cross-domain robustness underscores the potential of AstroSpy in broader applications, including medical imaging and forensic analysis.

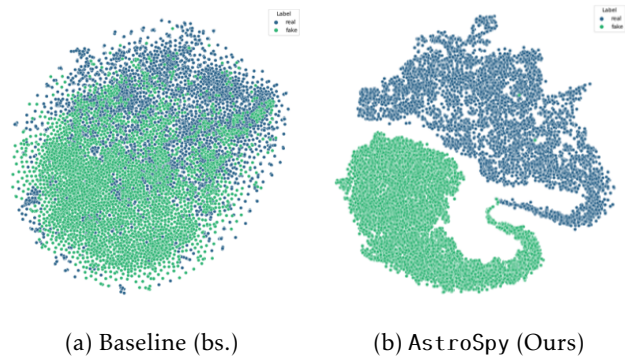


**Figure 2:** t-SNE visualization of the joint embeddings from AstroSpy. The plot shows distinct clusters for real (blue) and fake (green) images, indicating effective feature separation and the model’s ability to differentiate between real and generated astronomical images. Baseline indicates embeddings from Fourier Transformed embeddings.

### 3.4 Feature Shifts via AstroSpy

We employ t-SNE visualizations to analyze the feature shifts captured by AstroSpy. The embeddings show distinct clusters for real and fake images, validating the effectiveness of our joint feature representation. Figure 2 illustrates the t-SNE visualization of the joint embeddings. The distinct separation between real and fake images in the plot underscores the discriminative power of AstroSpy’s joint embeddings, reinforcing the model’s ability to effectively differentiate between real and generated astronomical images.

### 3.5 Qualitative Analysis

To understand the effectiveness of AstroSpy, we provide a qualitative analysis of real and synthetic images along with their spectra, as shown in Figure 3. Real

**Table 1:** Performance when trained on different embedding combinations. **Joint** indicates concatenated embeddings  $f_{joint}$ .

Configuration	In-Domain Real+Fake	Out-Of-Domain (OOD)				Average
		ImageNet	MIMIC	Fairface	OOD Average	
Fourier embeds (bs.)	0.69	0.59	0.55	0.51	0.55	0.58
Img embeds	0.89	0.64	0.50	0.70	0.61	0.68
Img embeds + Augs.	0.94	0.71	0.55	0.56	0.60	0.69
<b>Joint (AstroSpy)</b>	<b>0.98 ↑</b>	<b>0.83 ↑</b>	<b>0.59 ↑</b>	<b>0.93 ↑</b>	<b>0.78 ↑</b>	<b>0.83 ↑</b>

**Table 2:** Classification performance of AstroSpy when trained across different backbones.

Trained Backbone	In-Domain Real+Fake	Out-Of-Domain (OOD)				Average
		ImageNet	MIMIC	Fairface	OOD Average	
CNN	0.82	0.53	0.48	0.51	0.50	0.58
DenseNet121	0.96	0.71	0.55	0.82	0.69	0.76
<b>ResNet50</b>	<b>0.98 ↑</b>	<b>0.83 ↑</b>	<b>0.59 ↑</b>	<b>0.93 ↑</b>	<b>0.78 ↑</b>	<b>0.83 ↑</b>

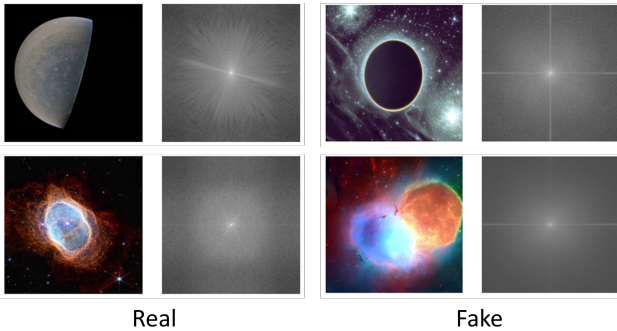


**Figure 3:** Samples of real (left column) and synthetic (right column) astronomical images with their corresponding spectra. The spectra reveal distinct patterns that help in differentiating real images from fakes.

images exhibit natural and continuous spectral patterns, indicative of genuine celestial structures. In contrast, synthetic images display spectral artifacts and frequency distributions due to generation processes.

- **Real Images and Spectra:** The real images show clear and detailed astronomical objects with well-defined frequency components and smooth gradients in their spectra, reflecting their authenticity.
- **Synthetic Images and Spectra:** The synthetic images mimic real astronomical appearances but lack intricate details and natural variations. Their spectra reveal artifacts and patterns, highlighting the limitations of generation models.

### 3.6 Impact of Data Augmentation

Table 3 summarizes the impact of different augmentation techniques on the model’s performance. The results demonstrate that individual augmentations such

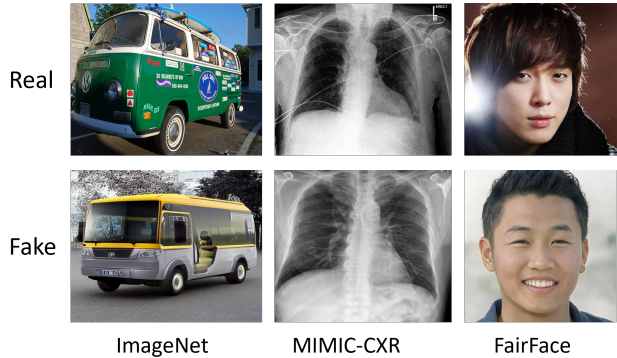


**Figure 4:** Samples of *out-of-domain* datasets used for testing AstroSpy’s generalization capabilities. The top row shows real images from a specific class, while the bottom row shows corresponding generated images.

as horizontal flip, color jitter, and random rotation significantly improve model performance compared to no augmentation. However, the combined application of all augmentation techniques yields the highest accuracy and F1-score, achieving 98% and 97%, respectively.

## 4 Conclusion

In this study, we introduced AstroSpy, a hybrid model that combines spatial and spectral features to distinguish real astronomical images from fakes, demonstrating superior performance. Using a unique dataset of real and synthetic images, AstroSpy effectively maintains the authenticity of astronomical data. Future work will explore AstroSpy’s robustness against sophisticated fake image generation processes, including commercial generators in out-of-domain analysis. We will also examine the potential misuse of AstroSpy by malicious actors to create more convinc-

**Table 3:** Impact of different augmentation approaches when training the AstroSpy detector.

Augmentation Type	Accuracy	F1-Score
No Augmentation	0.88	0.87
Horizontal Flip	0.93	0.92
Vertical Flip	0.89	0.88
Random Rotation	0.91	0.90
Color Jitter	0.94	0.93
Gaussian Blur	0.89	0.88
<b>Combined Augs.</b>	<b>0.98 ↑</b>	<b>0.97 ↑</b>

ing fakes, providing insights to strengthen detection methods and develop countermeasures. These efforts aim to enhance AstroSpy’s effectiveness and ensure scientific integrity and public trust.

## References

- Rafique, R. *et al.* Deep fake detection and classification using error-level analysis and deep learning. *Scientific Reports* **13**, 7422 (2023).
- Bird, J. J. & Lotfi, A. Cifake: Image classification and explainable identification of ai-generated synthetic images. *IEEE Access* (2024).
- Heidari, A., Jafari Navimipour, N., Dag, H. & Unal, M. Deepfake detection using deep learning methods: A systematic and comprehensive review. *Wiley Interdisciplinary Reviews: Data Mining and Knowledge Discovery* **14**, e1520 (2024).
- Yan, Z., Zhang, Y., Fan, Y. & Wu, B. *Ucf: Uncovering common features for generalizable deepfake detection in Proceedings of the IEEE/CVF International Conference on Computer Vision* (2023), 22412–22423.
- Shamshad, F., Srivatsan, K. & Nandakumar, K. *Evading Forensic Classifiers with Attribute-Conditioned Adversarial Faces in Proceedings of the IEEE/CVF Conference on Computer Vision and Pattern Recognition* (2023), 16469–16478.
- Nguyen, T. T. *et al.* Deep learning for deepfakes creation and detection: A survey. *Computer Vision and Image Understanding* **223**, 103525 (2022).
- Imam, R. & Alam, M. T. *Optimizing Brain Tumor Classification: A Comprehensive Study on Transfer Learning and Imbalance Handling in Deep Learning Models in International Workshop on Epistemic Uncertainty in Artificial Intelligence* (2023), 74–88.
- Hackstein, S., Kinakh, V., Bailer, C. & Melchior, M. Evaluation metrics for galaxy image generators. *Astronomy and Computing* **42**, 100685 (2023).
- Kim, J. J., Um, R. S., Lee, J. W. & Ajilore, O. Generative AI can fabricate advanced scientific visualizations: ethical implications and strategic mitigation framework. *AI and Ethics*, 1–13 (2024).
- Smith, M. J. & Geach, J. E. Astronomia ex machina: a history, primer and outlook on neural networks in astronomy. *Royal Society Open Science* **10**, 221454 (2023).
- Razzak, M. I., Naz, S. & Zaib, A. Deep learning for medical image processing: Overview, challenges and the future. *Classification in BioApps: Automation of decision making*, 323–350 (2018).
- Rana, M. S., Nobil, M. N., Murali, B. & Sung, A. H. Deepfake detection: A systematic literature review. *IEEE access* **10**, 25494–25513 (2022).
- Masood, M. *et al.* Deepfakes generation and detection: State-of-the-art, open challenges, countermeasures, and way forward. *Applied intelligence* **53**, 3974–4026 (2023).
- Farid, H. Image forgery detection. *IEEE Signal processing magazine* **26**, 16–25 (2009).
- Cozzolino, D., Poggi, G. & Verdoliva, L. *Splicebuster: A new blind image splicing detector in 2015 IEEE International Workshop on Information Forensics and Security (WIFS)* (2015), 1–6.
- Cheng, C., Zhang, L., Li, H., Dai, L. & Cui, W. A Deep Stochastic Adaptive Fourier Decomposition Network for Hyperspectral Image Classification. *IEEE Transactions on Image Processing* (2024).
- Durall, R., Keuper, M. & Keuper, J. *Watch your up-convolution: Cnn based generative deep neural networks are failing to reproduce spectral distributions in Proceedings of the IEEE/CVF conference on computer vision and pattern recognition* (2020), 7890–7899.
- Frank, J. *et al.* Leveraging frequency analysis for deep fake image recognition in *International conference on machine learning* (2020), 3247–3258.
- Alam, M. T., Imam, R., Guizani, M. & Karray, F. FLARE up your data: Diffusion-based Augmentation Method in *Astronomical Imaging*. *arXiv preprint arXiv:2405.13267* (2024).
- Bao, F. *et al.* One transformer fits all distributions in multi-modal diffusion at scale in *International Conference on Machine Learning* (2023), 1692–1717.
- Chambon, P. *et al.* Roentgen: Vision-language foundation model for chest x-ray generation. *arXiv preprint arXiv:2211.12737* (2022).
- Karras, T. *et al.* Analyzing and improving the image quality of stylegan in *Proceedings of the IEEE/CVF conference on computer vision and pattern recognition* (2020), 8110–8119.
- Bao, F. *et al.* One Transformer Fits All Distributions in Multi-Modal Diffusion at Scale 2023. *arXiv: 2303.06555 [cs.LG]*.
- He, K., Zhang, X., Ren, S. & Sun, J. *Deep residual learning for image recognition in Proceedings of the IEEE conference on computer vision and pattern recognition* (2016), 770–778.
- Duoandikoetxea, J. *Fourier analysis* (American Mathematical Society, 2024).
- Rombach, R., Blattmann, A., Lorenz, D., Esser, P. & Ommer, B. *High-resolution image synthesis with latent diffusion models in Proceedings of the IEEE/CVF conference on computer vision and pattern recognition* (2022), 10684–10695.
- Deng, J. *et al.* *Imagenet: A large-scale hierarchical image database in 2009 IEEE conference on computer vision and pattern recognition* (2009), 248–255.
- Johnson, A. E. *et al.* MIMIC-CXR-JPG, a large publicly available database of labeled chest radiographs. *arXiv preprint arXiv:1901.07042* (2019).
- Karkkainen, K. & Joo, J. *Fairface: Face attribute dataset for balanced race, gender, and age for bias measurement and mitigation in Proceedings of the IEEE/CVF winter conference on applications of computer vision* (2021), 1548–1558.
- Paszke, A. *et al.* Pytorch: An imperative style, high-performance deep learning library. *Advances in neural information processing systems* **32** (2019).